New Journal of Physics

The open access journal at the forefront of physics

PAPER

Doublon–holon pair creation in Mott–Hubbard systems in analogy to QED

F Queisser[1,2,*] , K Krutitsky[3], P Navez[4] and R Schützhold[1,2]

[1] Helmholtz-Zentrum Dresden-Rossendorf, Bautzner Landstraße 400, 01328 Dresden, Germany
[2] Institut für Theoretische Physik, Technische Universität Dresden, 01062 Dresden, Germany
[3] Fakultät für Physik, Universität Duisburg-Essen, Lotharstraße 1, 47057 Duisburg, Germany
[4] Department of Physics, Loughborough University, Loughborough LE11 3TU, United Kingdom
[*] Author to whom any correspondence should be addressed.

E-mail: f.queisser@hzdr.de

Abstract

Via the hierarchy of correlations, we study doublon–holon pair creation in the Mott state of the Fermi–Hubbard model (in higher dimensions) induced by a time-dependent electric field. Special emphasis is placed on the analogy to electron–positron pair creation from the vacuum in quantum electrodynamics. We find that the accuracy and applicability of this analogy depends on the spin structure of the Mott background. For Ising type anti-ferromagnetic order, we derive an effective Dirac equation. A Mott state without any spin order or spin polarized states do not explicitly display the same quasi-relativistic behavior.

1. Introduction

Non-equilibrium dynamics in strongly interacting quantum many-body systems is a rich and complex field displaying many fascinating phenomena. As the prototypical example of strongly interacting quantum many-body systems on a lattice, we consider the Mott insulator phase of the Fermi–Hubbard model [1, 2]. We assume that the system starts in equilibrium at half-filling, with on-site repulsion strong enough to prevent the fermions from hopping to the neighboring lattice sites. On top of this Mott insulator background state, we study the evolution of quasi-particle excitations in the form of doublons (doubly occupied sites) and holons (empty sites). A time-dependent electric field, e.g. induced by an incident optical laser, can then serve as the external stimulus driving the system out of equilibrium—leading to the creation of doublon–holon pairs, see also [3–8].

The intuitive similarity between the lower Hubbard band and the Dirac sea in quantum electrodynamics (QEDs) on the one hand and the upper Hubbard band and the positive energy continuum on the other hand suggests analogies between doublon–holon pair creation from the Mott state and electron–positron pair creation from the vacuum. Indeed, previous studies of the Fermi–Hubbard model in one spatial dimension have indicated such analogies on the qualitative as well as quantitative level, see, e.g. [7–9]. However, the behavior of the Fermi–Hubbard model in one dimension (where it is exactly solvable via the Bethe ansatz [10, 11]) is quite different from that in higher dimensions. For example, there is no transition from the metallic to the Mott insulating state at finite values of the hopping rate and the on-site repulsion [11]. In the following, we study the quantitative analogy between the Mott state of the Fermi–Hubbard model and QED in more detail, with special emphasis on the space-time dependence in more than one dimension, including the propagation of doublons and holons, and the spin structure. More specifically, we strive for an analytic understanding without mapping the Fermi–Hubbard Hamiltonian to an effective single-site model, see also [4, 12].

Of course, analogies between electron–positron pair creation in QED and other systems at lower energies have already been discussed in previous works. Examples include ultra-cold atoms in optical lattices [13–24]

as well as electrons in semi-conductors [25–27], graphene [28–46], or ^{3}He [47]. However, there are important differences to the Fermi–Hubbard model considered here: The Mott gap arises naturally through the interaction [1, 48] and the quantitative analogy to the 1+1 dimensional Dirac equation emerges without additional fine-tuning (at least in the case of Ising type spin order, see section 3). The particle-hole symmetry between the upper and lower Hubbard band—in analogy to the $\mathcal{C}$ symmetry in QED—is also an intrinsic property. In contrast, the valence and conduction bands in semi-conductors, for example, typically display different band structures, i.e. dispersion relations.

2. Extended Fermi–Hubbard model

In terms of the fermionic creation and annihilation operators $\hat{c}^\dagger_{\mu s}$ and $\hat{c}_{\nu s}$ at the lattice sites μ and ν with spin $s \in \{\uparrow, \downarrow\}$ and the associated number operators $\hat{n}_{\mu s}$, the extended Fermi–Hubbard Hamiltonian reads ($\hbar = 1$)

$$\hat{H} = -\frac{1}{Z}\sum_{\mu\nu s} T_{\mu\nu}\hat{c}^\dagger_{\mu s}\hat{c}_{\nu s} + U\sum_\mu \hat{n}^\uparrow_\mu \hat{n}^\downarrow_\mu + \sum_{\mu s} V_\mu \hat{n}_{\mu s}. \tag{1}$$

Here the hopping matrix $T_{\mu\nu}$ equals the tunneling strength T for nearest neighbors μ and ν and is zero otherwise. The coordination number Z counts the number of nearest neighbors μ for a given lattice site ν and is assumed to be large $Z \gg 1$. In order to describe the Mott insulator, the on-site repulsion U is also supposed to be large $U \gg T$. Finally, the potential $V_\mu(t)$ represents the external electric field, e.g. an optical laser.

The particle-hole symmetry between the upper and lower Hubbard band mentioned in the Introduction can be understood by interchanging all creation and annihilation operators $\hat{c}_{\mu s} \leftrightarrow \hat{c}^\dagger_{\mu s}$. Up to an irrelevant global shift of the chemical potential or the potential V_μ, this transformation $\hat{c}_{\mu s} \leftrightarrow \hat{c}^\dagger_{\mu s}$ maps the Fermi–Hubbard Hamiltonian (1) into the same form, but with T and V_μ changing their sign $T \to -T$ and $V_\mu \to -V_\mu$. For bi-partite lattices (see section 3), the sign change of T can be eliminated by a staggered phase transformation where the creation and annihilation operators of all odd lattice sites (i.e. within one sub-lattice) acquire an additional factor of -1.

2.1. Hierarchy of correlations

To obtain an approximate analytical solution, we consider the reduced density matrices of one $\hat{\rho}_\mu$ and two $\hat{\rho}_{\mu\nu}$ lattice sites etc. Next, we define the n-site correlators by subtracting all possible correlations involving $n-1$ sites or fewer from the reduced n-site matrix. For instance, the correlations between two lattice sites are

$$\hat{\rho}^{\mathrm{corr}}_{\mu\nu} = \hat{\rho}_{\mu\nu} - \hat{\rho}_\mu\hat{\rho}_\nu, \tag{2}$$

the general form of the correlators is discussed in appendix A. For large $Z \gg 1$, we may employ an expansion into powers of $1/Z$ where we find that higher-order correlators are successively suppressed [49–53]. More precisely, the two-point correlator scales as $\hat{\rho}^{\mathrm{corr}}_{\mu\nu} = \mathcal{O}(1/Z)$, while the three-point correlation is suppressed as $\hat{\rho}^{\mathrm{corr}}_{\mu\nu\lambda} = \mathcal{O}(1/Z^2)$, and analogously for higher orders.

Via this expansion into powers of $1/Z$, we may find approximate solutions of the evolution equations

$$i\partial_t\hat{\rho}_\mu = F_1\left(\hat{\rho}_\mu, \hat{\rho}^{\mathrm{corr}}_{\mu\nu}\right),$$
$$i\partial_t\hat{\rho}^{\mathrm{corr}}_{\mu\nu} = F_2\left(\hat{\rho}_\mu, \hat{\rho}^{\mathrm{corr}}_{\mu\nu}, \hat{\rho}^{\mathrm{corr}}_{\mu\nu\lambda}\right). \tag{3}$$

Using $\hat{\rho}^{\mathrm{corr}}_{\mu\nu} = \mathcal{O}(1/Z)$, the first evolution equation can be approximated by $i\partial_t\hat{\rho}_\mu = F_1(\hat{\rho}_\mu, 0) + \mathcal{O}(1/Z)$. Its zeroth-order solution $\hat{\rho}^0_\mu$ yields the mean-field background, which we will specify further in sections 3 and 4.

Next, the suppression $\hat{\rho}^{\mathrm{corr}}_{\mu\nu\lambda} = \mathcal{O}(1/Z^2)$ allows us to approximate the second equation (3) to leading order in $1/Z$ via $i\partial_t\hat{\rho}^{\mathrm{corr}}_{\mu\nu} \approx F_2(\hat{\rho}^0_\mu, \hat{\rho}^{\mathrm{corr}}_{\mu\nu}, 0)$. In order to solve this leading-order equation, it is convenient to split the fermionc creation and annihilation operators in particle $I=1$ and hole $I=0$ contributions via [54, 55]

$$\hat{c}_{\mu s I} = \hat{c}_{\mu s}\hat{n}^I_{\mu\bar{s}} = \begin{cases} \hat{c}_{\mu s}\left(1 - \hat{n}_{\mu\bar{s}}\right) & \text{for} \quad I=0 \\ \hat{c}_{\mu s}\hat{n}_{\mu\bar{s}} & \text{for} \quad I=1 \end{cases}, \tag{4}$$

where $\bar{s}$ denotes the spin opposite to s. In terms of these particle and hole operators, the correlations (for $\mu \neq \nu$) are (to leading order in $1/Z$) determined by

$$i\partial_t \langle \hat{c}^\dagger_{\mu sI} \hat{c}_{\nu sJ} \rangle^{\mathrm{corr}} = \frac{1}{Z} \sum_{\lambda L} T_{\mu\lambda} \langle \hat{n}^I_{\mu\bar{s}} \rangle^0 \langle \hat{c}^\dagger_{\lambda sL} \hat{c}_{\nu sJ} \rangle^{\mathrm{corr}}$$

$$- \frac{1}{Z} \sum_{\lambda L} T_{\nu\lambda} \langle \hat{n}^J_{\nu\bar{s}} \rangle^0 \langle \hat{c}^\dagger_{\mu sI} \hat{c}_{\lambda sL} \rangle^{\mathrm{corr}}$$

$$+ \left([J - I] U + V_\nu - V_\mu \right) \langle \hat{c}^\dagger_{\mu sI} \hat{c}_{\nu sJ} \rangle^{\mathrm{corr}}$$

$$+ \frac{T_{\mu\nu}}{Z} \left(\langle \hat{n}^I_{\mu\bar{s}} \rangle^0 \langle \hat{n}_{\nu s} \hat{n}^J_{\nu\bar{s}} \rangle^0 - \langle \hat{n}^J_{\nu\bar{s}} \rangle^0 \langle \hat{n}_{\mu s} \hat{n}^I_{\mu\bar{s}} \rangle^0 \right), \tag{5}$$

where $\langle \hat{X}_\mu \rangle^0 = \mathrm{Tr}\{\hat{X}_\mu \hat{\rho}^0_\mu\}$ denote expectation values in the zeroth-order mean-field background $\hat{\rho}^0_\mu$.

2.2. Factorization

The evolution equations (5) for the correlators can be simplified by factorizing them via the following effective linear equations for the particle and hole operators [56]

$$(i\partial_t - IU - V_\mu) \hat{c}_{\mu sI} = -\frac{1}{Z} \sum_{\nu J} T_{\mu\nu} \langle \hat{n}^I_{\mu\bar{s}} \rangle^0 \hat{c}_{\nu sJ}. \tag{6}$$

Of course, the hierarchy of correlations is not the only way to derive such effective evolution equations, similar results can be obtained by other approaches, such as the Hubbard-I approximation or similar mean-field approximation schemes, see, e.g. [1, 56–58]. One advantage of the scheme used here is that it allows for a clear separation between the leading and sub-leading contributions via a consistent expansion into powers of $1/Z$.

For example, in contrast to the dynamics of the charge modes in equations (5) and (6), the evolution of the spin fluctuations is much slower. The spin components $\hat{S}^i_\mu$ at the lattice site μ are given by $\hat{S}^i_\mu = \sum_{ss'} \hat{c}^\dagger_{\mu s} \sigma^i_{ss'} \hat{c}_{\mu s}/2$ in terms of the Pauli spin matrices $\sigma^i_{ss'}$. Deriving the rate of change of their correlations $i\partial_t \langle \hat{S}^i_\mu \hat{S}^j_\nu \rangle^{\mathrm{corr}}$ from equation (3), one finds that this time derivative is suppressed [55, 59] by an additional order of $1/Z$, see also equation (8) below. As a consequence, we may treat the evolution of the charge modes in equations (5) and (6) propagating on a mean-field background with a given (i.e. fixed) spin structure – which will be our approach in the next sections. This allows us to study the impact of the underlying spin structure.

To make this point more explicit, let us discuss the relevant time (or frequency) scales. As explained above, we find a hierarchy of energy (or frequency) scales. The largest relevant energy scale is the Mott gap $\sim U$. The next energy scale $\sim T/Z$ describes the hopping from one lattice site to another and is much smaller. Finally, the characteristic energy scale of the spin fluctuations is again much smaller $\sim T^2/(UZ^2)$, see also equation (8) below. In the following, we consider time scales which are short enough to neglect the spin dynamics, i.e. time scales much shorter than UZ^2/T^2. For example, the oscillation period of the external electric field could be in resonance with the Mott gap, i.e. an ultra-short time scale $\sim 1/U$. In order to facilitate the creation of doublon-holon pairs, the interaction time, e.g. the length of the optical laser pulse, could be in the intermediate regime $\sim Z/T$ (but still much shorter than UZ^2/T^2).

2.3. Comparison to other approaches

Since the method of the hierarchy of correlations employed here is based on the formal limit of large Z, it might be useful to compare it to other approaches which are also based on (or motivated by) this limit. A prominent example is dynamical mean-field theory (DMFT), see, e.g. [4, 60]. However, there are important differences between the two methods. While the hopping term in the Hamiltonian (1) scales with $1/Z$ in our approach, DMFT employs a scaling with $1/\sqrt{Z}$. As a result, the limit $Z \to \infty$ is already non-trivial in DMFT, whereas it is much simpler in our case because all correlations vanish. This simplicity allows us to calculate the $1/Z$-corrections around the zeroth-order mean-field background, where we also directly see the impact of the structure and dimensionality of the lattice. As another difference, DMFT usually employs numerical solution techniques whereas our approach is predominantly analytical.

Similar arguments apply to other mean-field type schemes such as the Gutzwiller ansatz, see [61, 62]. They typically employ a variational ansatz in order to approximate the solution within a highly restricted sub-set of states. Even though some of the obtained results might look similar, this method is clearly different from our approach based on a consistent and unambiguous expansion into powers of $1/Z$.

Going to the other extreme, the integrability of the Fermi–Hubbard model in one dimension via a Bethe ansatz [10, 11] facilitates approximate or even exact solutions. However, the behavior in one dimension (e.g. the character of the Mott transition) is very different from that in higher dimensions—such that one cannot directly compare these cases.
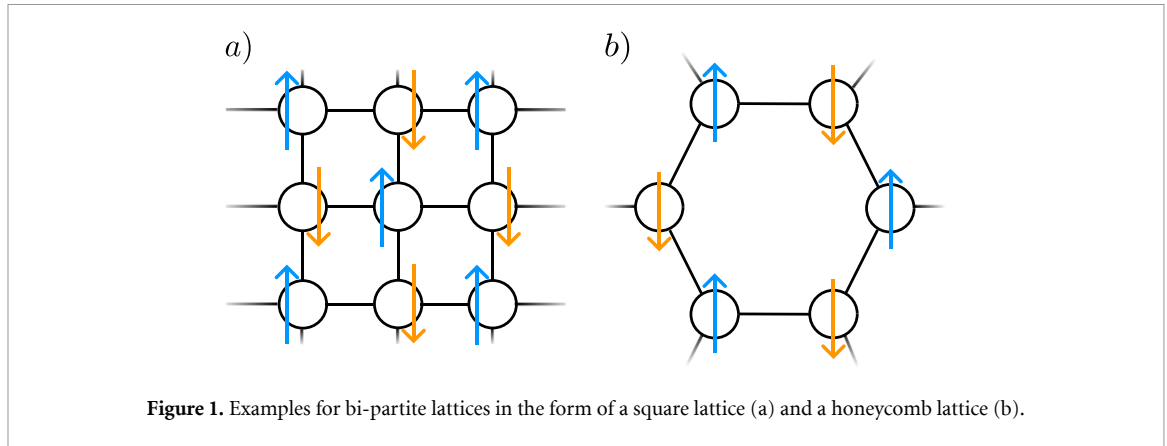
Figure 1. Examples for bi-partite lattices in the form of a square lattice (a) and a honeycomb lattice (b).

3. Ising type spin order

In order to analyze the effective equation (6), we have to specify the mean-field background $\hat{\rho}_{\mu}^{0}$. The Mott insulator state corresponds to having one particle per lattice site, which leaves to determine the remaining spin degrees of freedom. As our first example, we consider anti-ferromagnetic spin order of the Ising type [63]. To this end, we assume a bi-partite lattice which can be split into two sub-lattices $\mathcal{A}$ and $\mathcal{B}$ where all neighbors ν of a lattice site $\mu \in \mathcal{A}$ belong to $\mathcal{B}$ and vice versa, see also figure 1. Then, the zeroth-order mean-field background reads

$$\hat{\rho}_{\mu}^{0} = \begin{cases} |\uparrow\rangle_{\mu}\langle\uparrow| & \text{for} \quad \mu \in \mathcal{A} \\ |\downarrow\rangle_{\mu}\langle\downarrow| & \text{for} \quad \mu \in \mathcal{B} \end{cases} . \tag{7}$$

This state minimizes the Ising type anti-ferromagnetic interaction $\hat{S}_{\mu}^{z}\hat{S}_{\nu}^{z}$. Note that the Fermi–Hubbard Hamiltonian (1) does indeed generate an effective anti-ferromagnetic interaction via second-order hopping processes, but it would correspond to a Heisenberg type anti-ferromagnetic interaction [64]

$$\hat{H}_{\text{Heisenberg}} = \frac{4T^2}{Z^2 U} \sum_{<\mu\nu>} \hat{\mathbf{S}}_{\mu} \cdot \hat{\mathbf{S}}_{\nu} . \tag{8}$$

Although the state (7) does not describe the exact minimum of this interaction $\hat{\mathbf{S}}_{\mu} \cdot \hat{\mathbf{S}}_{\nu}$, it can be regarded as an approximation or a simplified toy model for such an anti-ferromagnet.

Alternatively, one could imagine additional spin interactions (stemming from the full microscopic description) which are not contained in the tight-binding model (1) and stabilize the state (7). For simplicity, in the following we assume that the state (7) is stabilized by a staggered magnetic field as described by the Hamiltonian

$$\hat{H}_{\text{staggered}} = \sum_{\mu s} \varepsilon_{\mu s} \hat{n}_{\mu s} , \tag{9}$$

where $\varepsilon_{\mu\uparrow} = -\varepsilon < 0$ and $\varepsilon_{\mu\downarrow} = \varepsilon$ in sub-lattice $\mathcal{A}$, and the other way around in sub-lattice $\mathcal{B}$. Since the strength of the Heisenberg type anti-ferromagnetic interaction (8) is suppressed by an additional factor of $1/Z$ and scales with T^2/U in the strong-coupling limit, we can choose a very small value of $\varepsilon \ll U$ such that the resulting modification to the dynamics of the doublons and holons is negligible, as will be illustrated in the subsequent section.

Going beyond this zeroth order (7), one could include the back-reaction of the correlations $\hat{\rho}_{\mu\nu}^{\text{corr}}$ by solving the evolution equation $i\partial_t \hat{\rho}_{\mu} = F_1(\hat{\rho}_{\mu}, \hat{\rho}_{\mu\nu}^{\text{corr}})$ from equation (3). This would be particularly important if many doublon-holon pairs are created because they would alter the mean-field background (7) significantly. Thus, the subsequent investigations based on equation (7) do only describe the onset of the dielectric breakdown of the Mott insulator state. Similarly, the creation of many doublon–holon pairs would eventually heat up the system and thus destroy the spin structure of the background (7).

3.1. Effective Dirac equation
The above background (7) supports hole excitations $I = 0$ of spin $\uparrow$ and particle excitations $I = 1$ of spin $\downarrow$ for the sub-lattice $\mathcal{A}$, and vice versa for the sub-lattice $\mathcal{B}$. For the other terms, such as $\hat{c}_{\mu \in \mathcal{A}, s=\uparrow, I=1}$, the

right-hand side of equation (6) vanishes and thus they become trivial and are omitted in the following, see appendix B.

As a result, particle excitations in the sub-lattice $\mathcal{A}$ are tunnel coupled to hole excitations of the same spin in the sub-lattice $\mathcal{B}$ and vice versa. Introducing the effective spinor in analogy to the Dirac equation

$$\hat{\psi}_{\mu \in \mathcal{A}} = \begin{pmatrix} \hat{c}_{\mu\downarrow I=1} \\ \hat{c}_{\mu\uparrow I=0} \end{pmatrix}, \quad \hat{\psi}_{\mu \in \mathcal{B}} = \begin{pmatrix} \hat{c}_{\mu\uparrow I=1} \\ \hat{c}_{\mu\downarrow I=0} \end{pmatrix}, \tag{10}$$

the evolution equation (6) can be cast into the form

$$i\partial_t \hat{\psi}_\mu = \begin{pmatrix} V_\mu + U & 0 \\ 0 & V_\mu \end{pmatrix} \cdot \hat{\psi}_\mu - \frac{1}{Z} \sum_\nu T_{\mu\nu} \sigma_x \cdot \hat{\psi}_\nu, \tag{11}$$

where σ_x is the Pauli spin matrix. This form is already reminiscent of the Dirac equation in 1+1 dimensions. To make the analogy more explicit, we first apply a simple phase transformation $\hat{\psi}_\mu \to \hat{\psi}_\mu \exp\{-itU/2\}$ after which the U term in equation (11) reads $\sigma_z U/2$.

Note that the staggered magnetic field (9) would only generate an additional term $\varepsilon \sigma_z \cdot \hat{\psi}_\mu$ in equation (11) which can simply be absorbed by a global shift of U and does not play any role here due to $\varepsilon \ll U$.

Since the wavelength of an optical laser is typically much longer than all other relevant length scales, we may approximate it (in the non-relativistic regime[5]) by a purely time-dependent electric field $\mathbf{E}(t)$ such that the potential reads $V_\mu(t) = q\mathbf{r}_\mu \cdot \mathbf{E}(t)$ where $\mathbf{r}_\mu$ is the position vector of the lattice site μ. In optics, this is usually referred to as the length gauge within the electric dipole approximation. Then we may use the Peierls transformation $\hat{\psi}_\mu \to \hat{\psi}_\mu \exp\{i\varphi_\mu(t)\}$ with $\dot{\varphi}_\mu = V_\mu$ to shift the potential V_μ into time-dependent phases of the hopping matrix $T_{\mu\nu} \to T_{\mu\nu}e^{i\varphi_\mu(t)-i\varphi_\nu(t)} = T_{\mu\nu}(t)$. Next, a spatial Fourier transformation simplifies equation (11) to

$$i\partial_t \hat{\psi}_{\mathbf{k}} = \left(\frac{U}{2}\sigma_z - T_{\mathbf{k}}(t)\sigma_x \right) \cdot \hat{\psi}_{\mathbf{k}}, \tag{12}$$

where $T_{\mathbf{k}}(t)$ denotes the Fourier transform of the hopping matrix including the time-dependent phases, which yields the usual minimal coupling form $T_{\mathbf{k}}(t) = T_{\mathbf{k}-q\mathbf{A}(t)}$. Note that the Peierls transformation is closely related to the gauge transformation $A_\mu \to A_\mu + \partial_\mu \chi$ in electrodynamics. Using this gauge freedom, one can represent an electric field $\mathbf{E}(t)$ via the scalar potential ϕ as $\partial_t + iq\phi$ in analogy to the V_μ or, alternatively, via the vector potential $\mathbf{A}$ as $\nabla - iq\mathbf{A}$ in analogy to the $T_{\mathbf{k}}(t) = T_{\mathbf{k}-q\mathbf{A}(t)}$.

In the absence of the electric field, $\mathbf{A} = 0$, the dispersion relation following from equation (12) reads

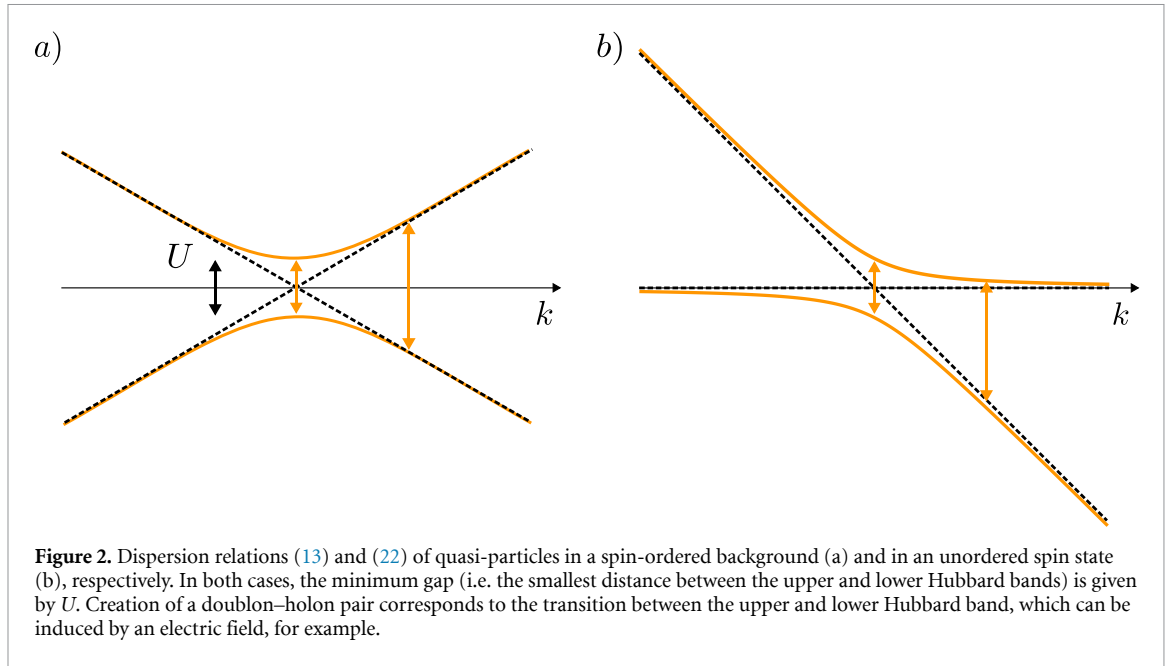$$\omega_{\mathbf{k}} = \pm \sqrt{\frac{U^2}{4} + T_{\mathbf{k}}^2}, \tag{13}$$

see also the illustration in figure 2(a). The positive and negative frequency solutions correspond to the upper and lower Hubbard bands, which are separated by the Mott gap. Unless the electric field is too strong or too fast, one expects the main contributions to doublon–holon pair creation near the minimum gap, i.e. the minimum of $T_{\mathbf{k}}^2$, typically at $T_{\mathbf{k}} = 0$. Then, a Taylor expansion $\mathbf{k} = \mathbf{k}_0 + \delta\mathbf{k}$ around a zero $\mathbf{k}_0$ of $T_{\mathbf{k}}$ yields $i\partial_t \hat{\psi}_{\mathbf{k}} \approx (U\sigma_z/2 - \mathbf{c}_{\mathrm{eff}} \cdot \delta\mathbf{k}\,\sigma_x) \cdot \hat{\psi}_{\mathbf{k}}$, where $\mathbf{c}_{\mathrm{eff}} = \nabla_{\mathbf{k}} T_{\mathbf{k}}|_{\mathbf{k}_0}$ denotes the effective propagation velocity, in analogy to the speed of light in QED. In the direction of $\mathbf{c}_{\mathrm{eff}}$, we thus observe a quantitative analogy to the relativistic Dirac equation (in 1+1 dimension) for small $\delta\mathbf{k}$, even though we started from a non-relativistic many-body system.

Re-introducing the electric field, an analogous Taylor expansion of equation (12) around the minimum gap reads

$$i\partial_t \hat{\psi}_{\mathbf{k}} \approx \left(\frac{U}{2}\sigma_z - \mathbf{c}_{\mathrm{eff}} \cdot [\delta\mathbf{k} - q\mathbf{A}(t)]\,\sigma_x \right) \cdot \hat{\psi}_{\mathbf{k}}, \tag{14}$$

as already expected from the minimal-coupling scheme discussed above. At first sight, the validity of this approximation (14) would require both, $\delta\mathbf{k}$ and $q\mathbf{A}(t)$, to be small. However, for strong and slowly varying

---

[5] In the non-relativistic approximation used here, the impact of the magnetic component of the laser is neglected because the characteristic velocities of the fermions in the optical lattice are much smaller than the speed of light c. Similarly, the coupling between the magnetic field and the spins of the fermions is omitted. Note that the real speed of light c is much larger than the effective speed of light $\mathbf{c}_{\mathrm{eff}}$ entering the effective Dirac equation (14). Therefore, the non-relativistic approximation used here does not contradict the quasi-relativistic behavior of the effective Dirac equation (14).

Figure 2. Dispersion relations (13) and (22) of quasi-particles in a spin-ordered background (a) and in an unordered spin state (b), respectively. In both cases, the minimum gap (i.e. the smallest distance between the upper and lower Hubbard bands) is given by U. Creation of a doublon–holon pair corresponds to the transition between the upper and lower Hubbard band, which can be induced by an electric field, for example.

electric fields, the term $q\mathbf{A}(t)$ could actually become quite large, e.g. comparable to the size of the Brillouin zone (in the regime of Bloch oscillations [65, 66]). Thus, one might expect that the approximation (14) breaks down in this situation, but fortunately this is not the case: Using the formal analogy of equation (12) to a Landau–Zener transition [67–69], we again see that doublon–holon pair creation occurs predominantly (unless the electric field is too strong or too fast) near the minimum of $T_{\mathbf{k}}(t)$ where we may apply the same Taylor expansion as before.

The only difference is that for large variations of $q\mathbf{A}(t)$, the pairs are no longer created near $\mathbf{k}_0$ in general, but also at other momenta $\mathbf{k} \approx \mathbf{k}_0 + q\mathbf{A}(t)$ where t is the approximate time of creation. The difference between $\mathbf{k}_0$ and $\mathbf{k}$ corresponds to the acceleration or deceleration of the doublons and holons after their creation. Hence, the number of created doublon–holon pairs can be calculated from the effective Dirac equation (14), but their final velocity may depend on the dispersion relation $T_{\mathbf{k}}$ away from $\mathbf{k}_0$. Similarly, due to Bloch oscillations, the minimum gap may be traversed several times, which can lead to interference effects of the associated pair-creation amplitudes. These effects correspond to multiple solutions of $\mathbf{k} \approx \mathbf{k}_0 + q\mathbf{A}(t)$ for different t but the same $\mathbf{k}$ caused by the periodicity of the dispersion relation $T_{\mathbf{k}}$ and are also not captured by the effective Dirac equation (14).

3.2. Analogy to QED

Up to simple phase factors $\exp\{\mathbf{k}_0 \cdot \mathbf{r}_\mu\}$, equation (14) displays a quantitative analogy to the Dirac equation in 1+1 dimensions, where c_{eff} plays the role of the speed of light while $U/2$ corresponds to the mass $m_{\text{eff}} c_{\text{eff}}^2 = U/2$. As a result, we may now apply many of the results known from QED [67–77] such as Klein tunneling [72] or the Sauter-Schwinger pair creation [73–75]. For example, the effective spinor $\hat{\psi}_{\mathbf{k}}$ can be expanded into particle and hole contributions (first in the absence of an electric field)

$$\hat{\psi}_{\mathbf{k}} = u_{\mathbf{k}} \hat{d}_{\mathbf{k}} + v_{\mathbf{k}} \hat{h}_{\mathbf{k}}^\dagger, \tag{15}$$

where the quasi-particles are usually referred to as doublons $\hat{d}_{\mathbf{k}}$ (upper Hubbard band) and holons $\hat{h}_{\mathbf{k}}^\dagger$ (lower Hubbard band). The Mott state $|\text{Mott}\rangle$ is then determined by $\hat{d}_{\mathbf{k}} |\text{Mott}\rangle = \hat{h}_{\mathbf{k}} |\text{Mott}\rangle = 0$.

In the presence of an electric field, these operators can mix – as described by the Bogoliubov transformation

$$\hat{d}_{\mathbf{k}}^{\text{out}} = \alpha_{\mathbf{k}} \hat{d}_{\mathbf{k}}^{\text{in}} + \beta_{\mathbf{k}} \left(\hat{h}_{\mathbf{k}}^{\text{in}} \right)^\dagger, \tag{16}$$

where the structure of the Dirac equation (14) implies the normalization $|\alpha_{\mathbf{k}}|^2 + |\beta_{\mathbf{k}}|^2 = 1$. Starting in the Mott state $\hat{d}_{\mathbf{k}}^{\text{in}} |\text{Mott}\rangle = \hat{h}_{\mathbf{k}}^{\text{in}} |\text{Mott}\rangle = 0$, the $\beta_{\mathbf{k}}$ coefficient yields the amplitude for doublon-holon pair creation $\hat{d}_{\mathbf{k}}^{\text{out}} |\text{Mott}\rangle \propto \beta_{\mathbf{k}}$.

In order to calculate the Bogoliubov coefficients, let us write the effective Dirac equation (14) in the form $i\partial_t \hat{\psi}_{\mathbf{k}} = \mathbf{M}_{\mathbf{k}} \cdot \hat{\psi}_{\mathbf{k}}$ in terms of a time-dependent 2×2 matrix $\mathbf{M}_{\mathbf{k}}$. The instantaneous eigenvalues of this matrix
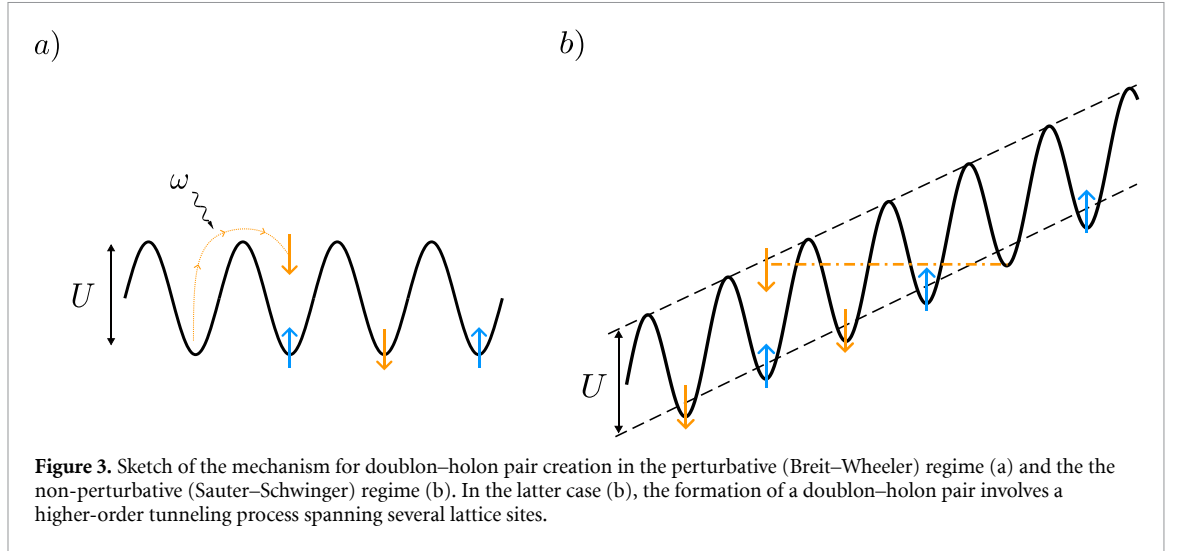
Figure 3. Sketch of the mechanism for doublon–holon pair creation in the perturbative (Breit–Wheeler) regime (a) and the the non-perturbative (Sauter–Schwinger) regime (b). In the latter case (b), the formation of a doublon–holon pair involves a higher-order tunneling process spanning several lattice sites.

are given by $\pm\omega_{\mathbf{k}}(t) = \pm\sqrt{U^2/4 + (\mathbf{c}_{\mathrm{eff}} \cdot [\delta\mathbf{k} - q\mathbf{A}(t)])^2}$ and correspond to the quasi-relativistic dispersion relation (13) around the minimum gap up to replacing the canonical momentum $\delta\mathbf{k}$ (which is conserved) by the mechanical momentum $\delta\mathbf{k} - q\mathbf{A}(t)$, which reflects the acceleration by the electric field. In the absence of an electric field, the eigenvectors of the matrix $\mathbf{M}_{\mathbf{k}}$ are the $u_{\mathbf{k}}$ and $v_{\mathbf{k}}$ in equation (15). If we add an electric field, the matrix $\mathbf{M}_{\mathbf{k}}(t)$ and thus also its eigenvectors become time-dependent $u_{\mathbf{k}}(t)$ and $v_{\mathbf{k}}(t)$. This leads to a mixing between the positive and negative frequency components (16), which in turn determines rate of the doublon-holon pair creation. In order to quantify this mixing, let us expand the solution $f_{\mathbf{k}}(t)$ of the effective Dirac equation $i\partial_t f_{\mathbf{k}} = \mathbf{M}_{\mathbf{k}} \cdot f_{\mathbf{k}}$ which initially coincides with the positive frequency solution $f_{\mathbf{k}}(t \to -\infty) = u_{\mathbf{k}}^{\mathrm{in}}$ into the instantaneous time-dependent $u_{\mathbf{k}}(t)$ and $v_{\mathbf{k}}(t)$ for arbitrary times

$$f_{\mathbf{k}}(t) = \alpha_{\mathbf{k}}(t)\, u_{\mathbf{k}}(t)\, e^{+iS_{\mathbf{k}}(t)} + \beta_{\mathbf{k}}(t)\, v_{\mathbf{k}}(t)\, e^{-iS_{\mathbf{k}}(t)}, \tag{17}$$

in terms of the time-dependent Bogoliubov coefficients $\alpha_{\mathbf{k}}(t)$ and $\beta_{\mathbf{k}}(t)$ and the phase function $S_{\mathbf{k}}(t)$ which satisfies $\dot{S}_{\mathbf{k}}(t) = \omega_{\mathbf{k}}(t) = \sqrt{U^2/4 + (\mathbf{c}_{\mathrm{eff}} \cdot [\delta\mathbf{k} - q\mathbf{A}(t)])^2}$. If we now consider the time-dependent ratio $R_{\mathbf{k}}(t) = \beta_{\mathbf{k}}(t)/\alpha_{\mathbf{k}}(t)$ of the Bogoliubov coefficients, we find that it satisfies the Riccati equation

$$\dot{R}_{\mathbf{k}}(t) = \frac{qU\mathbf{c}_{\mathrm{eff}} \cdot \mathbf{E}(t)}{2\omega_{\mathbf{k}}^2(t)} \left(e^{+2iS_{\mathbf{k}}(t)} + R_{\mathbf{k}}^2(t)\, e^{-2iS_{\mathbf{k}}(t)} \right). \tag{18}$$

Solving this Riccati equation with the initial condition $\dot{R}_{\mathbf{k}}(t \to -\infty) = 0$ yields the ratio of the Bogoliubov coefficients for all times. Together with their normalization $|\alpha_{\mathbf{k}}|^2 + |\beta_{\mathbf{k}}|^2 = 1$, this allows us to determine the pair-creation probability $|\beta_{\mathbf{k}}|^2$ per mode $\mathbf{k}$ in the final state as in equation (16).

Again, in complete analogy to QED, we may now discuss different regimes. First, we consider very weak electric fields $\mathbf{E}(t) = \mathbf{E}_0 \cos(\omega t)$ oscillating at some frequency ω. Then we find that $R_{\mathbf{k}}$ is also very small and thus we may neglect the second term $\propto R_{\mathbf{k}}^2$ in the Riccati equation (18). For the same reason (as in perturbation theory), we may approximate $\omega_{\mathbf{k}}^2(t)$ by the undisturbed expression (13) to lowest order. Thus we find resonant growth of $R_{\mathbf{k}}$ if the driving frequency ω matches twice the (undisturbed) mode frequency $2\omega_{\mathbf{k}}$, which implies $\omega \approx U$. As an intuitive picture, a fermion can absorb one photon from the external electric field and thereby gain enough energy to overcome the Mott gap and to form a doublon-holon pair by tunneling to the neighboring lattice site, see also figure 3(a). For this process, we find the usual lowest-order perturbative scaling $\beta_{\mathbf{k}} \sim |q\mathbf{c}_{\mathrm{eff}} \cdot \mathbf{E}_0|$, see, e.g. [78]. In QED, electron–positron pair creation by photons to lowest order perturbation theory is usually referred to as the Breit-Wheeler effect [78]. Note, however, that there is an important difference between the two cases: Electron–positron pair creation in vacuum QED requires two photons due to Lorentz invariance and energy-momentum conservation, where one has to take into account the dependence of the electromagnetic field on space *and* time. In our case, photons move much faster than the effective Dirac particles $c \gg |\mathbf{c}_{\mathrm{eff}}|$ such that the photon wavelengths are much longer (for the same frequency) and thus we may approximate them by purely time-dependent electric fields. In other words, the momentum of the absorbed photon is extremely small in comparison to the characteristic momenta of the fermions and does not play a role here. (Furthermore, it can also be absorbed by the whole lattice.)

Higher orders of perturbation theory then lead us in the multi-photon regime, for example $n\omega \approx U$ with $\beta_{\mathbf{k}} \sim |q\mathbf{c}_{\text{eff}} \cdot \mathbf{E}_0|^n$. Note that a completely different kind of resonances such as $\omega \approx 2U$ can occur if we take higher-order correlations into account [59, 79], but these are beyond our effective description (14).

If the electric field becomes stronger and slower, we enter the non-perturbative regime of the Sauter–Schwinger effect where the pair-creation amplitude displays an exponential scaling [80, 81], see also [3, 7, 8, 82–84]

$$\beta_{\mathbf{k}} \sim \exp\left\{ -\frac{\pi U^2}{8q|\mathbf{c}_{\text{eff}} \cdot \mathbf{E}_0|} \right\} . \tag{19}$$

In this regime, the generation of a particle-hole pair involves tunneling across several lattice sites, see figure 3(b). We may also understand this exponential scaling in terms of the Riccati equation (18). For the lowest-order resonance $\omega = 2\omega_{\mathbf{k}}$, the time integral of that equation used for deriving the final value of $R_{\mathbf{k}}$ exhibited a stationary phase along the real time axis. In the non-perturbative regime of the Sauter–Schwinger effect, this stationary phase along the real time axis is transformed to a saddle point in the complex plane where the imaginary part scales with the inverse of the electric field, see, e.g. [85]. In view of the exponential suppression of such oscillating time integrals when going to imaginary times, we can understand the exponential scaling (19).

The quantitative analogy to the Dirac equation even allows us to directly transfer further results from QED, for example the dynamically assisted Sauter–Schwinger effect, where pair creation by a strong and slowly varying electric field is enhanced by adding a weaker and faster varying field, see, e.g. [86] and [28, 87].

4. Unordered spin state

Let us compare our findings above to the case of a mean-field background without any spin order

$$\hat{\rho}_{\mu}^0 = \frac{|\uparrow\rangle_{\mu}\langle\uparrow| + |\downarrow\rangle_{\mu}\langle\downarrow|}{2} , \tag{20}$$

which could arise for a finite temperature which is too small to excite doublon–holon pairs but large enough to destroy the spin order. Another option could be a weak magnetic disorder potential or spin frustration.

In this case, we do not have to distinguish the two sub-lattices $\mathcal{A}$ and $\mathcal{B}$ and all lattice sites can support particle and hole excitations. Since the spin components $\uparrow$ and $\downarrow$ evolve independently of each other, we drop the spin index in the following and introduce the effective spinor in analogy to the Dirac equation as $\hat{\psi}_{\mu} = (\hat{c}_{\mu I=1}, \hat{c}_{\mu I=0})^{\mathrm{T}}$.

Because all expectation values $\langle \hat{n}_{\mu s}^I \rangle^0$ yield $1/2$ (instead of zero or unity), the analogue of equation (12) now reads (after the same phase transformation)

$$i\partial_t \hat{\psi}_{\mathbf{k}} = \frac{1}{2} \begin{pmatrix} U - T_{\mathbf{k}} & -T_{\mathbf{k}} \\ -T_{\mathbf{k}} & -U - T_{\mathbf{k}} \end{pmatrix} \cdot \hat{\psi}_{\mathbf{k}} . \tag{21}$$

The eigenvalues of the above 2×2-matrix yield the quasi-particle frequencies [1, 57]

$$\omega_{\mathbf{k}}^{\pm} = \frac{1}{2}\left(-T_{\mathbf{k}} \pm \sqrt{T_{\mathbf{k}}^2 + U^2} \right) , \tag{22}$$

which are depicted in figure 2(b). In view of the additional term $-T_{\mathbf{k}}$ in front of the square root, this dispersion relation does not display the same quasi-relativistic form as in equation (13). Putting it another way, we find that equation (21) is not formally equivalent to the Dirac equation (in 1+1 dimensions).

As a consequence, the propagation of quasi-particles in the two mean-field backgrounds (7) and (21) is quite different. For the Ising type order (7), the coherent propagation (without changing the background structure) of a doublon or holon (once they are created) requires second-order hopping processes see figure 4. Hence $\omega_{\mathbf{k}}$ in equation (13) is a quadratic function of $T_{\mathbf{k}}$. For the unordered background (20), on the other hand, doublons and holons can propagate coherently via first-order hopping processes, see figure 5. This is reflected in the linear contribution $-T_{\mathbf{k}}$ in equation (22), see appendix C.

However, if we do not consider quasi-particle propagation but focus on the probability for creating a doublon–holon pair in a given mode $\mathbf{k}$, we may again derive a close analogy to QED. To this end, we apply yet another $\mathbf{k}$-dependent phase transformation $\hat{\psi}_{\mathbf{k}} \to e^{i\vartheta_{\mathbf{k}}(t)}\hat{\psi}_{\mathbf{k}}$ with $\dot{\vartheta}_{\mathbf{k}}(t) = T_{\mathbf{k}}(t)/2$. Note that $T_{\mathbf{k}}(t)$ contains the vector potential $\mathbf{A}(t)$, i.e. the time integral of the electric field $\mathbf{E}(t)$. Thus, the phase $\vartheta_{\mathbf{k}}(t)$ involves an additional time integral, which makes it a even more non-local function of time. After this phase transformation, equation (21) becomes again formally equivalent to the Dirac equation in 1+1 dimensions, but now with the effective speed of light being reduced by a factor of two.
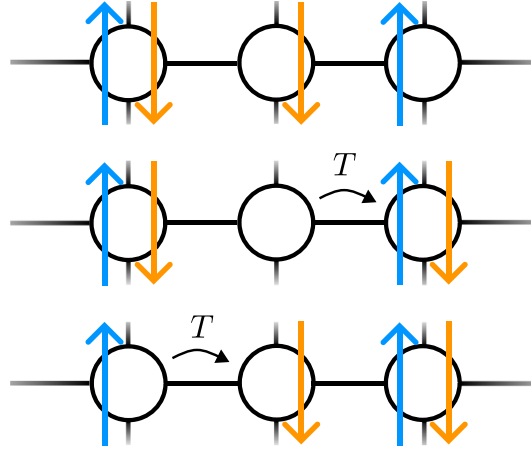
Figure 4. Sketch of the propagation of a doublon via a second-order hopping process. Due to the Pauli principle, the $\downarrow$ doublon sitting initially (top panel) on the left lattice site cannot tunnel to the middle site. Hence, first the fermion in the middle site has to tunnel to the right side (middle panel). Only as a second step, the $\downarrow$ fermion can leave the left site (bottom panel). As a result, the $\downarrow$ doublon effectively moved from the left to the right lattice site via a second-order hopping process.
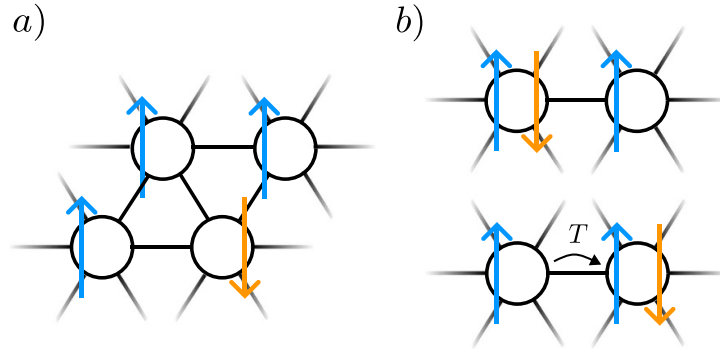

Figure 5. Triangular lattice (a) as an example for a lattice which is not bi-partite and hence does not admit perfect anti-ferromagnetic spin ordering due to frustration. In this case, a doublon can also propagate via a first-order hopping process (b).

5. Spin polarization

To investigate the impact of the spin structure of the mean-field background further, let us finally consider a spin polarized state with $\xi \in [0,1]$, see also [7, 9]

$$\hat{\rho}_\mu^0 = \xi \left|\uparrow\right\rangle_\mu \langle\uparrow| + (1-\xi) \left|\downarrow\right\rangle_\mu \langle\downarrow| . \tag{23}$$

Obviously, the spin components $\uparrow$ and $\downarrow$ will no longer behave in the same way, but their evolution equations are related to each other via the transformation $\xi \to 1-\xi$. Thus, we shall focus on the $\uparrow$ component in the following. The analogue of equation (21) then reads

$$i\partial_t \hat{\psi}_{\mathbf{k}} = \frac{1}{2} \begin{pmatrix} U - 2(1-\xi)T_{\mathbf{k}} & -2(1-\xi)T_{\mathbf{k}} \\ -2\xi T_{\mathbf{k}} & -U - 2\xi T_{\mathbf{k}} \end{pmatrix} \cdot \hat{\psi}_{\mathbf{k}} . \tag{24}$$

Note that, in contrast to equation (21), the above matrix is no longer unitary (unless $\xi = 1/2$) and thus special care is required for the normalization of the Bogoliubov coefficients, for example. Its eigenvalues are given by

$$\omega_{\mathbf{k}}^{\pm} = -\frac{T_{\mathbf{k}}}{2} \pm \frac{1}{2}\sqrt{T_{\mathbf{k}}^2 + U^2 + 2T_{\mathbf{k}}U(2\xi - 1)} . \tag{25}$$

In the fully polarized limits $\xi \to 0$ or $\xi \to 1$, they simply become $\omega_{\mathbf{k}}^+ = U/2 - T_{\mathbf{k}}$ and $\omega_{\mathbf{k}}^- = -U/2$ or $\omega_{\mathbf{k}}^+ = U/2$ and $\omega_{\mathbf{k}}^- = -U/2 - T_{\mathbf{k}}$, respectively. In this case, the square root in the dispersion relation, which was the hallmark of quasi-relativistic behavior, disappears. Furthermore, for $\xi \to 0$ doublons (with $\uparrow$) are

propagating according to $\omega_{\mathbf{k}}^+ = U/2 - T_{\mathbf{k}}$ while holons become trivial ($\omega_{\mathbf{k}}^- = -U/2$) whereas it is the other way around for $\xi \to 1$.

For $\xi \to 0$, the lower component in equation (24) just acquires an oscillating phase $\hat{c}_{\mathbf{k}\uparrow I=0}(t) = \hat{c}_{\mathbf{k}\uparrow I=0}^{\text{in}} e^{+iUt/2}$ and re-inserting this solution into equation (24), we find for the upper component

$$
\begin{aligned}
\hat{c}_{\mathbf{k}\uparrow I=1}^{\text{out}} &= \hat{c}_{\mathbf{k}\uparrow I=1}^{\text{in}} + \hat{c}_{\mathbf{k}\uparrow I=0}^{\text{in}} \int dt\, T_{\mathbf{k}}(t) \exp\{i\theta_{\mathbf{k}}(t)\} \\
&= \alpha_{\mathbf{k}} \hat{c}_{\mathbf{k}\uparrow I=1}^{\text{in}} + \beta_{\mathbf{k}} \hat{c}_{\mathbf{k}\uparrow I=0}^{\text{in}},
\end{aligned}
\tag{26}
$$

where $\dot{\theta}_{\mathbf{k}}(t) = U - T_{\mathbf{k}}(t)$. To estimate the above time integral, let us consider the specific example of a hyper-cubic lattice with lattice spacing ℓ in a constant electric field $\mathbf{E}$ aligned with one of the principal axes of the lattice, such that $T_{\mathbf{k}}(t) = T_{\mathbf{k}}^\perp + T\cos(k^\parallel \ell + qE\ell t)/Z$. Applying the saddle-point (or stationary-phase) method, we find saddle points at real times t_* if the electric field E is so strong that the electrostatic potential difference between neighboring sites (i.e. at a distance of ℓ) is large enough to overcome the Mott gap. However, for weaker electric fields $qE\ell \ll U$, i.e. the limit we are interested in, the saddle points t_* become complex and are given by $T_{\mathbf{k}}(t_*) \approx U$, i.e. $\text{Im}(t_*) \approx \pm(qE\ell)^{-1}\ln(2ZU/T)$.

Inserting this saddle point t_* into $\theta(t)$ allows us to estimate the exponential suppression of the Bogoliubov $\beta_{\mathbf{k}}$ coefficient in equation (26) via

$$
\beta_{\mathbf{k}} \sim \exp\left\{-\frac{U}{qE\ell}\ln\left(\frac{2ZU}{T}\right)\right\}.
\tag{27}
$$

Quite intuitively, we find that $\beta_{\mathbf{k}}$ is suppressed as $(T/U)^n$ where $n = U/(qE\ell)$ is the number of lattice sites after which the electrostatic potential difference is large enough to overcome the Mott gap $\approx U$, see also [88]. Similarly to the discussion in appendix C, nth order hopping processes are required to create doublon–holon pairs, such that the amplitude scales as $\beta_{\mathbf{k}} \sim (T/U)^n$.

Note, however, that we cannot directly relate $|\beta_{\mathbf{k}}|^2$ to doublon–holon pair creation since equation (24) is not analogous to the Dirac equation and thus the arguments in section 3.2 do not apply in the same way here. For example, in the case of perfect spin polarization $\xi = 0$, no pairs would be created at all. Doublon–holon pairs could be created if we have a small but non-zero spin minority $1 \gg \xi > 0$. To see that, let us imagine starting from the Mott state at zero hopping $T = 0$. Then we slowly switch on $T(t)$ before we apply the electric field. Afterwards, we slowly switch off $T(t)$ again and measure the occurrence of doublons, i.e. $\langle(\hat{c}_{\mathbf{k}\uparrow I=1}^{\text{out}})^\dagger \hat{c}_{\mathbf{k}\uparrow I=1}^{\text{out}}\rangle$. Inserting the Bogoliubov transformation (26), we find that this expectation value becomes $|\beta_{\mathbf{k}}|^2 \langle(\hat{c}_{\mathbf{k}\uparrow I=0}^{\text{in}})^\dagger \hat{c}_{\mathbf{k}\uparrow I=0}^{\text{in}}\rangle = |\beta_{\mathbf{k}}|^2 \xi$. Since $\xi \ll 1$, we may insert the estimate (27) of $\beta_{\mathbf{k}}$ at $\xi = 0$ to leading order in ξ.

6. Conclusions

We study doublon-holon pair creation from the Mott insulator state of the Fermi–Hubbard model induced by an external electric field $\mathbf{E}(t)$ which could represent an optical laser, for example. We find that the creation and propagation dynamics of the doublons and holons depends on the spin structure of the mean-field background. For Ising type anti-ferromagnetic order, we observe a quantitative analogy to QED. More specifically, in the vicinity of the minimum gap (i.e. the most relevant region for pair creation), the doublons and holons are described by an effective Dirac equation in 1+1 dimensions in the presence of an electric field $\mathbf{E}(t)$, see table 1.

As in most cases, the benefits of such an analogy are two-fold. On the one hand, it allows us to understand doublon–holon pair creation in the Fermi–Hubbard model better (see also the next paragraph). On the other hand, laboratory systems (e.g. fermionic atoms in optical lattices [89] or strongly interacting electrons in solids) which can be described by the Fermi–Hubbard model to a good approximation facilitate an experimental approach (via the analogy) to electron–positron pair creation in QED (where an experimental realization is much harder). For example, one could study the robustness of the Sauter–Schwinger effect, e.g. how much it is affected by the coupling to some environment. More generally, the transfer of ideas across the boundaries of sub-disciplines can be very fruitful ans sometimes yields unexpected results.

As a consequence of this quantitative analogy, we may employ the machinery of QED and apply many results regarding electron–positron pair creation to our set-up. For example, in the perturbative (single- or multi-photon) regime with the threshold conditions $\omega \geqslant nU$ for the nth order, the doublon–holon pair creation amplitude $\beta_{\mathbf{k}}$ yields the perturbative scaling $\beta_{\mathbf{k}} \sim |q\mathbf{c}_{\text{eff}} \cdot \mathbf{E}|^n$.

For stronger and slower electric fields, we enter the non-perturbative (tunneling) regime in analogy to the Sauter–Schwinger effect in QED and thus recover the exponential dependence already discussed earlier

Table 1. Sketch of the analogy. The electric field $\mathbf{E}(t)$ and elementary charge q play the same role in both cases.

Mott insulator	QED vacuum
Upper Hubbard band	Positive energy continuum
Lower Hubbard band	Dirac sea
Doublons & holons	Electrons & positrons
Mott gap $U = 2m_{\text{eff}}c_{\text{eff}}^2$	Electron mass
Velocity $\mathbf{c}_{\text{eff}} = \nabla_{\mathbf{k}} T_{\mathbf{k}}\vert_{\mathbf{k}_0}$	Speed of light c
Landau–Zener tunneling	Sauter–Schwinger effect
Peierls transformation	Gauge transformation

regarding the dielectric breakdown of Mott insulator, see, e.g. [4]. Note that the quantitative analogy established above (see also table 1) unambiguously determines the pair-creation exponent and pre-factor without any free fitting parameters.

If we consider the annihilation of doublon–holon pairs instead of their creation, this analogy applies to the stimulated annihilation within an external field, but not to the spontaneous annihilation of an electron–positron pair by emitting a pair of photons, for example. In order to model this process, one has to include a mechanism for dissipating the energy, e.g. by coupling the Fermi–Hubbard model to an environment, see also [51, 90–93].

For a mean-field background without any spin order, on the other hand, the creation and propagation of doublons and holons does not display such a quasi-relativistic behavior. The dispersion relation is different and the evolution equation deviates from the Dirac equation. Still, for a purely time-dependent electric field $\mathbf{E}(t)$ considered here, the doublon-holon pair creation amplitude $\beta_{\mathbf{k}}$ for a given mode $\mathbf{k}$ can again be related to QED. After a $\mathbf{k}$-dependent phase transformation (which is non-local in time), the amplitude $\beta_{\mathbf{k}}$ is given by the same expression, just with the effective speed of light c_{eff} being reduced by a factor of two. Note, however, that an additional factor of two in the exponent can imply a huge difference in the pair-creation probability. Furthermore, in view of the $\mathbf{k}$-dependence of the phase transformation, this mapping does only work for purely time-dependent electric field $\mathbf{E}(t)$. For space-time dependent electric fields $\mathbf{E}(t, \mathbf{r})$, the deviation of the dispersion relation and the resulting difference in propagation become important—which will be the subject of further studies.

Finally, a spin-polarized mean-field background deviates even further from the quasi-relativistic behavior discussed above. In the limit of nearly perfect spin polarization, for example, the doublon–holon pair creation exponent scales with $U \ln U$ for weak electric fields E instead of U^2 as in the quasi-relativistic case. It might be illuminating to compare these scalings with the Fermi–Hubbard model in one dimension, which is integrable and can be solved exactly via the Bethe ansatz [10, 11]. For this integrable system, different scalings of the pair-creation exponent with U^2, $U \ln U$ and $U^{3/2}$ have been obtained in various limiting cases [3, 7–9, 82–84]. Note, however, that one should be careful when comparing these results directly to our findings since the behavior in one dimension is qualitatively different from the case of higher dimensions studied here [10, 11]. Nevertheless, a common feature is that scalings with U^2 are found in quasi-relativistic cases while other scalings (such as $U \ln U$) correspond to non-relativistic behavior.

Having obtained such a distinctive dependence on the spin structure of the background, it should also be interesting to investigate other spin structures. For example, regarding the propagation of doublons and holons, the Heisenberg type anti-ferromagnetic spin structure can be regarded as lying somewhere in between the extremal cases of the Ising type anti-ferromagnet and the fully unordered spin state, see also [55]. Thus, one would expect that the results for the creation of doublon–holon pairs in the Heisenberg type background should also lie somewhere in between these two extremal cases. This should be the subject of future studies.

Data availability statement

All data that support the findings of this study are included within the article (and any supplementary files).

Acknowledgments

Appendix A. Hierarchy of correlations

The general form of the correlators can be derived via the generating functional

$$\mathcal{F}(\hat{\alpha}) = \mathcal{F}(\{\hat{\alpha}_\mu\}) = \ln\left[\text{tr}\left\{\hat{\rho}\bigotimes_\mu\left(\mathbf{1}_\mu + \hat{\alpha}_\mu\right)\right\}\right], \tag{A.1}$$

where $\hat{\rho}$ is the density matrix of the full lattice and the operator

$$\hat{\alpha}_\mu = \sum_{m,n}\alpha_\mu^{m,n}|m\rangle_\mu\langle n| \tag{A.2}$$

acts solely on the Hilbert space of the lattice site μ. Employing this functional, one can obtain all correlations via successive derivatives w.r.t. $\hat{\alpha}_\mu$ which are defined as

$$\frac{\partial\mathcal{F}(\{\alpha\})}{\partial\hat{\alpha}_\mu} = \sum_{m,n}|n\rangle_\mu\langle m|\frac{\partial\mathcal{F}(\{\alpha\})}{\partial\alpha_\mu^{m,n}}. \tag{A.3}$$

Thus, for a generals set $\mathcal{S} = \{\mu_1,\ldots,\mu_\ell\}$ of ℓ different lattice sites $\mu_1 \neq \cdots \neq \mu_\ell$, the correlation operators are determined by

$$\hat{\rho}_\mathcal{S}^{\text{corr}} = \frac{\partial}{\partial\hat{\alpha}_{\mu_1}}\frac{\partial}{\partial\hat{\alpha}_{\mu_2}}\cdots\frac{\partial}{\partial\hat{\alpha}_{\mu_\ell}}\mathcal{F}(\hat{\alpha})\bigg|_{\hat{\alpha}=0}. \tag{A.4}$$

The relation to the corresponding reduced density matrix operator $\rho_\mathcal{S} = \text{Tr}_{\mu\neq\mathcal{S}}(\hat{\rho})$ is given by

$$\hat{\rho}_\mathcal{S} = \hat{\rho}_{\mu_1\ldots\mu_\ell} = \sum_{\cup_i\mathcal{P}_i=\mathcal{S}}\prod_i\hat{\rho}_{\mathcal{P}_i}^{\text{corr}}. \tag{A.5}$$

For example, the three-point correlators are expressed as

$$\hat{\rho}_{\mu\nu\lambda}^{\text{corr}} = \hat{\rho}_{\mu\nu\lambda} - \hat{\rho}_{\mu\nu}^{\text{corr}}\hat{\rho}_\lambda - \hat{\rho}_{\mu\lambda}^{\text{corr}}\hat{\rho}_\nu - \hat{\rho}_{\nu\lambda}^{\text{corr}}\hat{\rho}_\mu - \rho_\mu\rho_\nu\rho_\lambda, \tag{A.6}$$

Employing the von-Neumann equation of the total density matrix, one can derive the time temporal evolution of the functional $\mathcal{F}$. By taking successive derivatives w.r.t. the operators $\hat{\alpha}_\mu$ one obtains the evolution equations for the correlations. Further details can be found in [53].

Appendix B. Generalized parity

In order to detail how one can separate the relevant operators $\hat{c}_{\mu sI}$ in equation (7) from the irrelevant ones, let us introduce the multi-index $A = \{\mu, s, I\}$. Then we may associate natural numbers $|\mu| \in \mathbb{N}$ to lattice sites μ such that $|\mu|$ is even for $\mu \in \mathcal{A}$ and odd for $\mu \in \mathcal{B}$. Similarly, we map the spin s to a natural number $|s|$ such that $|s| = 0$ for $\downarrow$ and $|s| = 1$ for $\uparrow$. Combining these numbers, we may define $|A| = |\mu| + |s| + I$.

This combined number allows us to characterize the mean-field background (6), for which we have $\langle\hat{n}_A\rangle^0 = 1$ for even $|A|$ and $\langle\hat{n}_A\rangle^0 = 0$ for odd $|A|$. If we now cast equation (4) into the general form

$$\mathrm{i}\partial_t\langle\hat{c}_A^\dagger\hat{c}_B\rangle^{\text{corr}} = \sum_C\Gamma_{AC}\langle\hat{c}_C^\dagger\hat{c}_B\rangle^{\text{corr}} + \bar{\Gamma}_{BC}\langle\hat{c}_A^\dagger\hat{c}_C\rangle^{\text{corr}} + \Xi_{AB}, \tag{B.1}$$

we see that non-zero source terms Ξ_{AB} only exist if both $|A|$ and $|B|$ are odd. Furthermore, the mixing matrices Γ_{AC} and $\bar{\Gamma}_{BC}$ are only non-vanishing if $|A|$ and $|B|$ are odd, respectively.

As a consequence, we only need to keep the correlators $\langle\hat{c}_A^\dagger\hat{c}_B\rangle^{\text{corr}}$ where both $|A|$ and $|B|$ are odd. The remaining correlators $\langle\hat{c}_A^\dagger\hat{c}_B\rangle^{\text{corr}}$ can be omitted if $|A|$ or $|B|$ or both are even. For those, the source terms Ξ_{AB} vanish and they are also not seeded by the odd–odd correlators due to the aforementioned property of the mixing matrices Γ_{AC} and $\bar{\Gamma}_{BC}$. Thus, they stay zero throughout the evolution, provided that they vanish initially (e.g. in an initial state where the hopping rate is switched off).

Appendix C. Strong-coupling perturbation theory

It might be illuminating to compare our results to strong-coupling perturation theory—both, for the stationary case as well as for the temporal evolution, see also [55]. To this end, we write the Hamiltonian (1) without the electric field (i.e. $V_\mu = 0$) in the form

$$\hat{H} = \hat{H}_U + \hat{H}_T = \hat{H}_0 + \hat{H}_1 \,, \tag{C.1}$$

and perform a power series expansion in terms of the small ratio $\varepsilon = T/U \ll 1$, e.g. for the Mott state

$$|\text{Mott}\rangle = |\text{Mott}\rangle_0 + \varepsilon |\text{Mott}\rangle_1 + \mathcal{O}\left(\varepsilon^2\right) \,. \tag{C.2}$$

Note that the first-order hopping corrections read

$$\varepsilon |\text{Mott}\rangle_1 = -\frac{\hat{H}_1}{U} |\text{Mott}\rangle_0 \,. \tag{C.3}$$

After studying the stationary case, let us now turn to the propagation of a doublon, for example. (Due to the particle-hole duality mentioned in the Introduction, holons behave basically in the same way.) First, let us consider three lattice sites displaying Ising-type spin order as in equation (6)

$$|\text{Mott}\rangle_0 = \ldots |\!\downarrow\rangle_1 |\!\uparrow\rangle_2 |\!\downarrow\rangle_3 \ldots \,. \tag{C.4}$$

A state corresponding to one doublon with spin $\uparrow$ can be created by inserting an additional fermion on the first lattice site

$$|\text{in}\rangle_0 = \ldots |\!\uparrow\downarrow\rangle_1 |\!\uparrow\rangle_2 |\!\downarrow\rangle_3 \ldots \,. \tag{C.5}$$

Due to Pauli blocking, this doublon cannot propagate to the second lattice site. Instead, the motion of this doublon (on a fixed spin background) requires a second-order hopping process where first the fermion from the second lattice site tunnels to the third

$$\hat{H}_1 |\text{in}\rangle_0 \propto \ldots |\!\uparrow\downarrow\rangle_1 |0\rangle_2 |\!\uparrow\downarrow\rangle_3 \ldots + \ldots \,, \tag{C.6}$$

reaching an intermediate state with higher energy, and then the double occupancy of the first site is dispersed by another hopping process

$$|\text{out}\rangle_0 = \ldots |\!\uparrow\rangle_1 |\!\downarrow\rangle_2 |\!\uparrow\downarrow\rangle_3 \ldots \,. \tag{C.7}$$

Effectively, this second-order hopping process moves the doublon from the first to the third lattice site.

On the other hand, a mean-field background without Ising-type spin order such as $|\text{Mott}\rangle_0 = \ldots |\!\downarrow\rangle_1 |\!\downarrow\rangle_2 \ldots$ would allow a doublon with spin $\uparrow$ on first lattice site $|\text{in}\rangle_0 = \ldots |\!\uparrow\downarrow\rangle_1 |\!\downarrow\rangle_2 \ldots$ to tunnel directly to the second lattice site $|\text{out}\rangle_0 = \ldots |\!\downarrow\rangle_1 |\!\uparrow\downarrow\rangle_2 \ldots$.

The above picture shows that the quasi-particle propagation is quite different in the two cases (6) and (15). This is reflected in the difference between the dispersion relations (10) and (17) where the former (10) starts quadratically in T while the latter (17) starts linearly.

ORCID iD

F Queisser ⬤ https://orcid.org/0000-0001-7378-0851

References

[1] Hubbard J 1963 Electron correlations in narrow energy bands *Proc. R. Soc. Lond.* A **276** 238
[2] Arovas D P, Berg E, Kivelson S A and Raghu S 2022 The Hubbard model *Annu. Rev. Condens. Matter Phys.* **13** 275
[3] Oka T, Arita R and Aoki H 2003 Breakdown of a Mott insulator: a nonadiabatic tunneling mechanism *Phys. Rev. Lett.* **91** 066406
[4] Eckstein M, Oka T and Werner P 2010 Dielectric breakdown of Mott insulators in dynamical mean-field theory *Phys. Rev. Lett.* **105** 146404
[5] Avigo I, Queisser F, Zhou P, Ligges M, Rossnagel K, Schützhold R and Bovensiepen U 2020 Doublon bottleneck in the ultrafast relaxation dynamics of hot electrons in 1T-TaS$_2$ *Phys. Rev. Res.* **2** 022046(R)
[6] Ligges M *et al* 2018 Ultrafast doublon dynamics in photoexcited 1T-TaS$_2$ *Phys. Rev. Lett.* **120** 166401
[7] Oka T and Aoki H 2005 Ground-state decay rate for the Zener breakdown in band and Mott insulators *Phys. Rev. Lett.* **95** 137601
[8] Oka T and Aoki H 2010 Dielectric breakdown in a Mott insulator: many-body Schwinger-Landau-Zener mechanism studied with a generalized Bethe ansatz *Phys. Rev.* B **81** 033103
[9] Lenarčič Z and Prelovšek P 2012 Dielectric breakdown in spin-polarized Mott insulator *Phys. Rev. Lett.* **108** 196401

[10] Essler F H L, Frahm H, Göhmann F, Klümper A and Korepin V E 2005 *The One-Dimensional Hubbard Model* (Cambridge University Press)

[11] Lieb E H and Wu F Y 1968 Absence of Mott transition in an exact solution of the short-range, one-band model in one dimension *Phys. Rev. Lett.* **20** 1445

[12] Georges A and Kotliar G 1992 Hubbard model in infinite dimensions *Phys. Rev. B* **45** 6479

[13] Piñeiro A M, Genkina D, Lu M and Spielman I B 2019 Sauter-Schwinger effect with a quantum gas *New J. Phys.* **21** 083035

[14] Witthaut D, Salger T, Kling S, Grossert C and Weitz M 2011 Effective Dirac dynamics of ultracold atoms in bichromatic optical lattices *Phys. Rev. A* **84** 033601

[15] Cirac J I, Maraner P and Pachos J K 2010 Cold atom simulation of interacting relativistic quantum field theories *Phys. Rev. Lett.* **105** 190403

[16] Zhu S-L, Wang B and Duan L-M 2007 Simulation and detection of Dirac fermions with cold atoms in an optical lattice *Phys. Rev. Lett.* **98** 260402

[17] Hou J-M, Yang W-X and Liu X-J 2009 Massless Dirac fermions in a square optical lattice *Phys. Rev. A* **79** 043621

[18] Lim L-K, Smith C M and Hemmerich A 2008 Staggered-vortex superfluid of ultracold bosons in an optical lattice *Phys. Rev. Lett.* **100** 130402

[19] Boada O, Celi A, Latorre J I and Lewenstein M 2011 Dirac equation for cold atoms in artificial curved spacetimes *New J. Phys.* **13** 035002

[20] Goldman N, Kubasiak A, Bermudez A, Gaspard P, Lewenstein M and Martin-Delgado M A 2009 Non-Abelian optical lattices: anomalous quantum Hall effect and Dirac fermions *Phys. Rev. Lett.* **103** 035301

[21] Kasper V, Hebenstreit F, Oberthaler M and Berges J 2016 Schwinger pair production with ultracold atoms *Phys. Lett. B* **760** 742

[22] Queisser F, Navez P and Schützhold R 2012 Sauter-Schwinger-like tunneling in tilted Bose-Hubbard lattices in the Mott phase *Phys. Rev. A* **85** 033625

[23] Szpak N and Schützhold R 2012 Optical lattice quantum simulator for quantum electrodynamics in strong external fields: spontaneous pair creation and the Sauter–Schwinger effect *New J. Phys.* **14** 035001

[24] Szpak N and Schützhold R 2011 Quantum simulator for the Schwinger effect with atoms in bichromatic optical lattices *Phys. Rev. A* **84** 050101(R)

[25] Linder M F, Lorke A and Schützhold R 2018 Analog Sauter-Schwinger effect in semiconductors for spacetime-dependent fields *Phys. Rev. B* **97** 035203

[26] Smolyansky S A, Tarakanov A V and Bonitz M 2009 Vacuum particle creation: analogy with the Bloch theory in solid state physics *Contrib. Plasma Phys.* **49** 575

[27] Hrivnák Ĺ 1993 Relativistic analogies in direct-gap semiconductors *Prog. Quantum Electr.* **17** 235

[28] Villalba-Chávez S, Mathiak O, Egger R and Müller C 2023 Light-amplified Landau-Zener conductivity in gapped graphene monolayers: a simulacrum of photocatalyzed vacuum instability *Phys. Rev. D* **108** 116007

[29] Dóra B and Moessner R 2010 Nonlinear electric transport in graphene: quantum quench dynamics and the Schwinger mechanism *Phys. Rev. B* **81** 165431

[30] Gavrilov S P, Gitman D M and Yokomizo N 2012 Dirac fermions in strong electric field and quantum transport in graphene *Phys. Rev. D* **86** 125022

[31] Allor D, Cohen T D and McGady D A 2008 Schwinger mechanism and graphene *Phys. Rev. D* **78** 096009

[32] Akal I, Egger R, Müller C and Villalba-Chávez S 2016 Low-dimensional approach to pair production in an oscillating electric field: application to bandgap graphene layers *Phys. Rev. D* **93** 116006

[33] Katsnelson M I and Volovik G E 2012 Quantum electrodynamics with anisotropic scaling: Heisenberg-Euler action and Schwinger pair production in the bilayer graphene *JETP Lett.* **95** 411

[34] Novoselov K S, Geim A K, Morozov S V, Jiang D, Katsnelson M I, Grigorieva I V, Dubonos S V and Firsov A A 2005 Two-dimensional gas of massless Dirac fermions in graphene *Nature* **438** 197

[35] Katsnelson M I, Novoselov K S and Geim A K 2006 Chiral tunnelling and the Klein paradox in graphene *Nat. Phys.* **2** 620

[36] Cheianov V V and Fal'ko V I 2006 Selective transmission of Dirac electrons and ballistic magnetoresistance of $n-p$ junctions in graphene *Phys. Rev. B* **74** 041403(R)

[37] Vandecasteele N, Barreiro A, Lazzeri M, Bachtold A and Mauri F 2010 Current-voltage characteristics of graphene devices: interplay between Zener-Klein tunneling and defects *Phys. Rev. B* **82** 045416

[38] Beenakker C W J 2008 Colloquium: Andreev reflection and Klein tunneling in graphene *Rev. Mod. Phys.* **80** 1337

[39] Fillion-Gourdeau F and MacLean S 2015 Time-dependent pair creation and the Schwinger mechanism in graphene *Phys. Rev. B* **92** 035401

[40] Sonin E B 2009 Effect of Klein tunneling on conductance and shot noise in ballistic graphene *Phys. Rev. B* **79** 195438

[41] Rosenstein B, Lewkowicz M, Kao H C and Korniyenko Y 2010 Ballistic transport in graphene beyond linear response *Phys. Rev. B* **81** 041416(R)

[42] Kao H C, Lewkowicz M and Rosenstein B 2010 Ballistic transport, chiral anomaly and emergence of the neutral electron-hole plasma in graphene *Phys. Rev. B* **82** 035406

[43] Kumar R K 2023 Mesoscopic Schwinger effect *Nat. Phys.* **19** 768

[44] Schmitt A *et al* 2023 Mesoscopic Klein-Schwinger effect in graphene *Nat. Phys.* **19** 830

[45] Shytov A, Rudner M, Gu N, Katsnelson M and Levitov L 2009 Atomic collapse, Lorentz boosts, Klein scattering and other quantum-relativistic phenomena in graphene *Solid State Commun.* **149** 1087

[46] Semenoff G W 1984 Condensed-matter simulation of a three-dimensional anomaly *Phys. Rev. Lett.* **53** 2449

[47] Schopohl N and Volovik G E 1992 Schwinger pair production in the orbital dynamics of ^{3}He-B *Ann. Phys., NY* **215** 372

[48] Mott N F 1949 The basis of the electron theory of metals, with special reference to the transition metals *Proc. Phys. Soc. A* **62** 416

[49] Navez P and Schützhold R 2010 Emergence of coherence in the Mott-insulator–superfluid quench of the Bose-Hubbard model *Phys. Rev. A* **82** 063603

[50] Krutitsky K V, Navez P, Queisser F and Schützhold R 2014 Propagation of quantum correlations after a quench in the Mott-insulator regime of the Bose-Hubbard model *EPJ Quantum Technol.* **1** 12

[51] Queisser F and Schützhold R 2019 Environment-induced prerelaxation in the Mott-Hubbard model *Phys. Rev. B* **99** 155110

[52] Navez P, Queisser F and Schützhold R 2016 Large-coordination-number expansion of a lattice Bose gas at finite temperature *Phys. Rev. A* **94** 023629

[53] Queisser F, Krutitsky K V, Navez P and Schützhold R 2014 Equilibration and prethermalization in the Bose-Hubbard and Fermi-Hubbard models *Phys. Rev. A* **89** 033616

[54] Navez P, Queisser F and Schützhold R 2014 Quasi-particle approach for lattice Hamiltonians with large coordination numbers *J. Phys. A: Math. Theor.* **47** 225004

[55] Queisser F, Schaller G and Schützhold R 2023 Attraction versus repulsion between doublons or holons in Mott-Hubbard systems *Int. J. Theor. Phys.* **62** 239

[56] Tsuji N and Werner P 2013 Nonequilibrium dynamical mean-field theory based on weak-coupling perturbation expansions: application to dynamical symmetry breaking in the Hubbard model *Phys. Rev.* B **88** 165115

[57] Herrmann T and Nolting W 1997 Magnetism in the single-band Hubbard model *J. Magn. Magn. Mater.* **170** 253

[58] Mancini F and Avella A 2004 The Hubbard model within the equations of motion approach *Adv. Phys.* **53** 537

[59] Queisser F and Schützhold R 2019 Boltzmann relaxation dynamics in the strongly interacting Fermi-Hubbard model *Phys. Rev.* A **100** 053617

[60] Georges A, Kotliar G, Krauth W and Rozenberg M J 1996 Dynamical mean-field theory of strongly correlated fermion systems and the limit of infinite dimensions *Rev. Mod. Phys.* **68** 13

[61] Ogawa T, Kanda K and Matsubara T 1975 Gutzwiller approximation for antiferromagnetism in Hubbard model *Prog. Theor. Phys.* **53** 614

[62] Gutzwiller M C 1963 Effect of correlation on the ferromagnetism of transition metals *Phys. Rev. Lett.* **10** 159

[63] Hirsch J E and Tang S 1989 Antiferromagnetism in the two-dimensional Hubbard model *Phys. Rev. Lett.* **62** 591

[64] Chao K A, Spałek J and Oleś A M 1978 Canonical perturbation expansion of the Hubbard model *Phys. Rev.* B **18** 3453

[65] Eckstein M and Werner P 2011 Damping of Bloch oscillations in the Hubbard model *Phys. Rev. Lett.* **107** 186406

[66] Niu Q, Zhao X-G, Georgakis G A and Raizen M G 1996 Atomic Landau-Zener tunneling and Wannier-Stark ladders in optical potentials *Phys. Rev. Lett.* **76** 4504

[67] Zener C 1932 Non-adiabatic crossing of energy levels *Proc. R. Soc.* A **137** 696

[68] Zener C 1934 A theory of the electrical breakdown of solid dielectrics *Proc. R. Soc.* A **145** 523

[69] Landau L D 1932 On the theory of transfer of energy at collisions II *Phys. Z. Sow.* **2** 46

[70] Dirac P A M 1928 The quantum theory of the electron *Proc. R. Soc.* A **117** 610

[71] Dirac P A M 1928 The quantum theory of the Electron. Part II *Proc. R. Soc.* A **118** 351

[72] Klein O 1929 Die Reflexion von Elektronen an einem Potentialsprung nach der relativistischen Dynamik von Dirac *Z. Phys.* **53** 157

[73] Sauter F 1932 Zum „Kleinschen Paradoxon" *Z. Phys.* **73** 547

[74] Heisenberg W and Euler H 1936 Folgerungen aus der Diracschen Theorie des Positrons *Z. Phys.* **98** 714

[75] Bunkin F V and Tugov I I 1970 Possibility of creating electron-positron pairs in a vacuum by the focusing of laser radiation *Sov. Phys. - Dokl.* **14** 678

[76] Nikishov A I and Ritus V I 1967 Ionization of atoms by an electromagnetic wave field *Sov. Phys. - JETP* **25** 1135

[77] Keldysh L V 1965 Ionization in the field of a strong electromagnetic wave *Sov. Phys. - JETP* **20** 1307

[78] Breit G and Wheeler J A 1934 Collision of two light quanta *Phys. Rev.* **46** 1087

[79] Queisser F, Schreiber S, Kratzer P and Schützhold R 2019 Boltzmann relaxation dynamics of strongly interacting spinless fermions on a lattice *Phys. Rev.* B **100** 245110

[80] Sauter F 1931 Über das Verhalten eines Elektrons im homogenen elektrischen Feld nach der relativistischen Theorie Diracs *Zeitschrift für Physik* **69** 742

[81] Schwinger J 1951 On gauge invariance and vacuum polarization *Phys. Rev.* **82** 664

[82] Heidrich-Meisner F, González I, Al-Hassanieh K A, Feiguin A E, Rozenberg M J and Dagotto E 2010 Nonequilibrium electronic transport in a one-dimensional Mott insulator *Phys. Rev.* B **82** 205110

[83] Tanaka Y and Yonemitsu K 2011 Crossover from bias-induced to field-induced breakdown in one-dimensional band and Mott insulators attached to electrodes *Phys. Rev.* B **83** 085113

[84] Takasan K, Nakagawa M, Kawakami N 2019 Dielectric breakdown of strongly correlated insulators in one dimension: universal formula from non-Hermitian sine-Gordon theory (arXiv:1908.06107)

[85] Linder M F, Schneider C, Sicking J, Szpak N and Schützhold R 2015 Pulse shape dependence in the dynamically assisted Sauter-Schwinger effect *Phys. Rev.* D **92** 085009

[86] Schützhold R, Gies H and Dunne G 2008 Dynamically assisted Schwinger mechanism *Phys. Rev. Lett.* **101** 130404

[87] Dunne G V, Gies H and Schützhold R 2009 Catalysis of Schwinger vacuum pair production *Phys. Rev.* D **80** 111301(R)

[88] Oka T 2012 Nonlinear doublon production in a Mott insulator: Landau-Dykhne method applied to an integrable model *Phys. Rev.* B **86** 075148

[89] Schützhold R 2025 Ultra-cold atoms as quantum simulators for relativistic phenomena (arXiv:2501.03785)

[90] Buča B and Prosen T 2017 Charge and spin current statistics of the open Hubbard model with weak coupling to the environment *Phys. Rev.* E **95** 052141

[91] Kleinherbers E, Szpak N, König J and Schützhold R 2020 Relaxation dynamics in a Hubbard dimer coupled to fermionic baths: phenomenological description and its microscopic foundation *Phys. Rev.* B **101** 125131

[92] Amaricci A, Weber C, Capone M and Kotliar G 2012 Approach to a stationary state in a driven Hubbard model coupled to a thermostat *Phys. Rev.* B **86** 085110

[93] Li J, Aron C, Kotliar G and Han J E 2015 Electric-field-driven resistive switching in the dissipative Hubbard model *Phys. Rev. Lett.* **114** 226403